

# PO-Flow: Flow-based Generative Models for Sampling Potential Outcomes and Counterfactuals

Dongze Wu\*, David I. Inouye†, Yao Xie\*

## Abstract

We propose PO-Flow, a novel continuous normalizing flow (CNF) framework for causal inference that jointly models potential outcomes and counterfactuals. Trained via flow matching, PO-Flow provides a unified framework for individualized potential outcome prediction, counterfactual predictions, and uncertainty-aware density learning. Among generative models, it is the first to enable density learning of potential outcomes without requiring explicit distributional assumptions (e.g., Gaussian mixtures), while also supporting counterfactual prediction conditioned on factual outcomes in general observational datasets. On benchmarks such as ACIC, IHDP, and IBM, it consistently outperforms prior methods across a range of causal inference tasks. Beyond that, PO-Flow succeeds in high-dimensional settings, including counterfactual image generation, demonstrating its broad applicability.

## 1 Introduction

Predicting potential outcomes (POs) lies at the core of causal inference. In a typical setting, each individual has two potential outcomes:  $Y^{(1)}$  if they receive a treatment ( $A = 1$ ) and  $Y^{(0)}$  if they do not ( $A = 0$ ). However, in the real world, only one outcome is observed, while the other potential outcome remains fundamentally unknown [28]. Accurately estimating both POs is crucial for decision-making in domains such as healthcare [41, 27, 50], where clinicians may wish to compare a patient’s likely outcomes under different treatment options [60, 20].

In the causal inference literature, the vast majority of methods focus on estimating the average treatment effect (ATE) and the conditional average treatment effect (CATE) at the population level [32, 25, 1, 22, 37, 42, 55, 67]. It is important to note that although some methods perform well in estimating population-level CATE, they may underperform in individualized potential outcome (PO) prediction, as accurately predicting POs in finite samples is challenging [52].

However, making decisions for individuals based on average treatment effects can be misleading. Therefore, accurately predicting individualized POs and learning their full distributions with uncertainty is a crucial task [69, 35]. Recent works [67, 44, 45] have explored generative models to sample POs and estimate empirical distributions. However, methods that learn the full density of POs without relying on explicit distributional assumptions (e.g., Gaussian mixtures) remain scarce.

In addition, another critical challenge is estimating the counterfactual outcome conditioned on the factual—that is, predicting what would have happened under the alternative treatment, given the observed outcome. This task is especially relevant in post-hoc clinical analyses, where practitioners ask, “Would the patient have fared better on another therapy?” [66, 29, 21].

\*H. Milton Stewart School of Industrial and Systems Engineering, Georgia Institute of Technology, Atlanta, GA 30332. <dwu381@gatech.edu> <yao.xie@isye.gatech.edu>

†Elmore Family School of Electrical and Computer Engineering, Purdue University, West Lafayette, IN 47907. <dinouye@purdue.edu>

Counterfactual prediction differs from standard PO estimation—it requires reasoning about outcomes under an alternative treatment *conditioned on the observed outcome*, introducing dependencies between observed and unobserved outcomes. Structural Causal Models (SCMs) [48] and modern extensions [46, 6, 13, 7, 65, 49, 9] offer the most widely used theoretical framework for counterfactual reasoning. SCMs methods typically assume known causal structures or aim to learn them explicitly. Yet, it may be possible to estimate counterfactuals directly without recovering the SCM [70]. In PO-Flow, we do not explicitly assume an SCM, but seek to directly estimate counterfactual outcomes.

We aim to develop a generative modeling framework that jointly supports population-level CATE estimation, individualized PO prediction with density modeling, and counterfactual outcome prediction without explicitly modeling an SCM—an area that has been relatively less explored.

## 1.1 Related Works

*CATE Estimation:* Numerous methods have been proposed for CATE estimation [32, 25, 1, 22, 37, 42, 55, 67]. Broadly, these fall into model-agnostic and model-specific approaches. Model-agnostic estimators, or meta-learners [37, 15, 16, 2, 54], typically follow one of two strategies [43]: (a) one-step methods, which fit regression models and compute CATE as the difference in predicted outcomes, and (b) two-step methods, which estimate nuisance functions to construct pseudo-outcomes, then regress them on covariates.

In contrast, model-specific estimators adapt machine learning techniques for CATE estimation, including methods such as [14, 55, 42, 34, 67]. More recently, neural networks have been widely applied to this task, with notable examples in [55, 42, 67]. However, most of these approaches mainly focus on estimating CATE rather than predicting individualized potential outcomes.

*Individualized POs Prediction:* Although some CATE methods can be adapted for potential outcomes (POs) prediction, they may perform suboptimally, particularly on finite samples, as they are not specifically optimized for accurate PO estimation. This limitation partly arises because many methods assume that CATE has a simpler functional structure than POs. Nevertheless, several CATE approaches are also designed with POs prediction as the target [37, 55, 67, 42, 45, 43], and these will serve as our primary baselines for experimental comparisons.

*Counterfactual Outcomes Prediction:* Structural Causal Models (SCMs) provide a well-established framework for counterfactual reasoning [48, 46, 6, 13, 7, 65, 49, 9], but practical applications often require specifying the full causal graph and structural equations, which may be difficult or infeasible for real-world data. Some recent works avoid explicitly modeling SCMs [39, 5, 44, 62], but typically address specific tasks and rely on additional information, such as temporal structure.

Some works [27, 34, 42, 38, 67] targeting CATE estimation describe their goal as counterfactual inference. However, in these works, "counterfactual" typically refers to the unobserved potential outcome under an alternative treatment, without conditioning on the observed factual outcome.

While SCMs offer theory-grounded counterfactual reasoning, general-purpose methods for individualized counterfactual prediction—without explicitly modeling SCMs or relying on auxiliary information—remain scarce. Although [67, 43] were not originally designed for counterfactuals, we adapt them by incorporating factual information into intermediate steps and use them as baselines.

*Diffusion and Flow Models:* Diffusion models [26, 57, 58] and flow-based generative models [12, 64, 40, 4] have demonstrated strong performance across a range of applications, including image generation, statistical sampling [18, 59, 61], and physics-informed modeling [8, 68, 51].

Recently, diffusion and flow-based generative models have been applied to causal inference tasks such as counterfactual image generation [53, 19], causal query answering [10], and inference over causal graphs or structural causal models [9, 33].

However, to our knowledge, only two generative algorithms have been proposed specifically for the potential outcomes (PO) task: the diffusion-based DiffPO [43] and the discrete normalizing flow-based INFs [45]. We conduct extensive comparisons with both methods in this work.

## 1.2 Main Contributions

We propose PO-Flow, a continuous normalizing flow (CNF) framework for potential outcomes and counterfactuals. Our **main contributions** are: (1) PO-Flow provides a unified generative framework for potential outcome prediction, CATE estimation, and general-purpose counterfactual prediction—without explicitly modeling structural causal models (SCMs) or relying on auxiliary information for the counterfactual task; (2) PO-Flow enables learning the density of predicted potential outcomes, offering deeper insights into uncertainty; (3) PO-Flow outperforms state-of-the-art methods across a range of causal tasks on multiple benchmarks.

## 2 Preliminaries

### 2.1 Neural ODE and Continuous Normalizing Flow:

A Neural ODE is a continuous model where the trajectory of data is modeled as the solution of an ordinary differential equation (ODE). Formally, in  $\mathbb{R}^d$ , given an input  $y_0 = y(0)$  at time  $t = 0$ , the transformation to the output  $y_1 = y(1)$  at time  $t = 1$  is governed by:

$$\frac{dy(t)}{dt} = v_\theta(y(t), t), \quad t \in [0, 1], \quad (1)$$

where  $v_\theta : \mathbb{R}^{d_Y+1} \rightarrow \mathbb{R}^{d_Y}$  represents the velocity field, which is parameterized by a neural network with parameter  $\theta$ . The time horizon is rescaled to  $[0, 1]$  without loss of generality.

Continuous Normalizing Flow (CNF) is a class of normalizing flows in which the transformation of a probability density is governed by a time-continuous Neural ODE. The marginal density of  $y(t)$ , denoted as  $p(y, t)$ , evolves according to the continuity equation implied by the ODE in Eq. (1). This continuity equation is given by:

$$\partial_t p(y, t) + \nabla \cdot (p(y, t)v_\theta(y, t)) = 0, \quad t \in [0, 1], \quad (2)$$

where  $\nabla \cdot$  denotes the divergence operator.

When the Neural ODE is well-posed, it defines a continuous and invertible mapping from the initial sample  $y_0$  to the terminal sample  $y_1$ . The inverse mapping from  $y_1$  to  $y_0$  can be computed by integrating the ODE (1) in reverse time. This framework allows setting  $y_0 \sim p(\cdot, 0)$  as the data distribution and  $y_1 \sim p(\cdot, 1)$  as the base (noise) distribution, typically chosen as  $N(0, I)$ .

For notational convenience, we define  $p_Y(\cdot) := p(\cdot, 0)$  as the data distribution and  $q(\cdot) := p(\cdot, 1)$  as the base (noise) distribution. Throughout this paper, we adopt the common choice  $q(\cdot) = N(0, I)$ .

### 2.2 Flow Matching

Flow Matching (FM) [40, 4] provides a simulation-free approach for training continuous normalizing flows by directly regressing the model velocity  $v_\theta(y, t)$  onto a predefined target velocity field  $u(y, t)$ . The original FM objective is defined as:

$$\mathcal{L}_{\text{FM}}(\theta) = \mathbb{E}_{t \sim \mathcal{U}[0, 1], y \sim p(\cdot, t)} [\|v_\theta(y, t) - u(y, t)\|^2], \quad (3)$$

where  $u(y, t)$  is an analytically specified target velocity field.

**Linear Interpolant:** Due to the intractability of  $u(y, t)$  without conditioning on the initial data  $y_0$ , Conditional Flow Matching (CFM) is introduced. Conditioned on an observed sample  $y_0 \sim p_Y(\cdot)$ , CFM employs a pre-specified interpolation function  $I_t$  between two endpoints  $y_0$  and  $y_1 \sim q(\cdot)$ , where  $q$  is typically  $N(0, I)$ . The interpolated path is defined as:

$$\phi_t := I_t(y_0, y_1), \quad t \in [0, 1]. \quad (4)$$

Here,  $I_t$  can be analytically specified. Conditioned on  $y_0$ , the optimal and most information-preserving choice is the linear interpolation path [40]:

$$\phi_t = (1 - t)y_0 + (t + \sigma_{\min}(1 - t))y_1, \quad (5)$$

where  $y_1 \sim N(0, I)$  and  $\sigma_{\min}$  is a small positive hyperparameter that ensures  $p(\phi_t, 0) \sim N(y_0, \sigma_{\min}^2 I)$ . When  $\sigma_{\min} = 0$ , this reduces to the strict linear interpolant  $\phi_t = (1 - t)y_0 + ty_1$ .

Here,  $\phi_t$  serves as a pre-specified reference trajectory that the ODE solution  $y(t)$  should follow at time  $t$ . Under the linear interpolant defined in (5), the corresponding reference velocity field becomes:

$$\frac{d\phi_t}{dt} = (1 - \sigma_{\min})y_1 - y_0. \quad (6)$$

**Training loss:** CFM trains the flow  $v_\theta(y(t), t)$  by directly regressing it onto the reference velocity field (6). The training objective is given by:

$$\mathcal{L}_{\text{CFM}}(\theta) = \mathbb{E}_{t \sim \mathcal{U}[0, 1], y_0 \sim p_Y(\cdot), y_1 \sim q(\cdot)} \|v_\theta(\phi_t, t) - \frac{d\phi_t}{dt}\|^2. \quad (7)$$

### 3 Problem Settings

**Notations and Setups:** We consider a setting where each individual is described by covariates  $X \in \mathbb{R}^{d_X}$ , a treatment assignment  $A \in \{0, 1\}$ , and an outcome  $Y^{(A)} \in \mathbb{R}^{d_Y}$  under treatment  $A$ . The observational dataset is  $\mathcal{D} = \{(y_i^{(a)}, x_i, a_i)\}_{i=1}^n \sim p_{Y, X, A}(\cdot)$ , where  $y_i^{(a)}$  is the observed potential outcome under treatment  $a_i$ , and  $(x_i, a_i) \sim p_{X, A}(\cdot)$  are the associated covariates and treatment.

**Potential Outcomes:** In the potential outcomes framework, each individual has two potential outcomes:  $Y^{(0)}$  (control) and  $Y^{(1)}$  (treatment), but only one is observed based on assignment  $A$ . We define potential outcome prediction as estimating  $Y^{(a)} \mid X, A = a$ . For convenience, we denote  $Y^{(a)}$  and  $\hat{Y}^{(a)}$  as the true and predicted potential outcomes.

**Counterfactual Outcomes:** In contrast to potential outcomes, we define the counterfactual outcome as  $Y_{\text{cf}}^{(1-a)} := Y^{(1-a)} \mid X, A = a, Y^{(a)}$ : the outcome had the individual received the opposite treatment, conditioned on its observed potential (factual) outcome. For convenience, we denote  $Y_{\text{cf}}^{(1-a)}$  and  $\hat{Y}_{\text{cf}}^{(1-a)}$  as the true and predicted counterfactual outcomes, respectively.

To ensure the identifiability of potential outcomes, we adopt the standard assumptions commonly used in the literature [43, 45, 67]:

**Assumption 3.1.** (1) Consistency: If an individual receives treatment  $A = a$ , the observed outcome equals the corresponding potential outcome:  $Y = Y^{(a)}$ . (2) Unconfoundedness: All confounders are observed, i.e.,  $\{Y^{(0)}, Y^{(1)}\} \perp\!\!\!\perp A \mid X$ . (3) Overlap: Treatment assignment is probabilistic:  $0 < P(A = 1 \mid X = x) < 1$ , for all  $x \in \mathcal{X}$ .

Counterfactuals are rarely identifiable without strong assumptions [63, 47]. Estimating them can often be framed as an optimal transport problem [11, 17]. To constrain the space of joint transport mappings, our PO-Flow framework introduces the following assumption, applicable only to Section 4.2:

**Assumption 3.2.** There exists a deterministic and invertible mapping  $f : \mathbb{R}^{d_Y+d_X} \times \{0, 1\} \rightarrow \mathbb{R}^{d_Z}$  that encodes the observed outcome as  $Z_Y = f(Y^{(A)}, X, A)$ . A counterfactual latent representation can be obtained as  $Z'_Y = Z_Y + \delta$ , where  $\delta \sim \mathcal{N}(0, \Sigma(X))$  is an optional covariate-dependent noise term. The counterfactual is then recovered via  $Y_{\text{cf}}^{(1-A)} = f^{-1}(Z'_Y, X, 1 - A)$ .

## 4 PO-Flow: A Continuous Normalizing Flow for Potential Outcomes

We introduce PO-Flow, a continuous normalizing flow framework for modeling potential and counterfactual outcomes, with three main goals: 1. predicting individualized potential outcomes, 2. estimating counterfactual outcomes, and 3. learning the densities.

Our PO-Flow framework is built on Continuous Normalizing Flows (CNFs) and is trained using the Flow Matching (FM) objective. Our learning target is the trajectory of the sample  $y(t)$  over  $t \in [0, 1]$ . To condition the dynamics on both covariates  $x$  and treatment  $a$ , our Neural ODE is defined as:

$$\frac{dy(t)}{dt} = v_\theta(y(t), t, x, a), \quad t \in [0, 1], \quad (8)$$

where  $v_\theta : \mathbb{R}^{d_Y+d_X+2} \rightarrow \mathbb{R}^{d_Y}$  is parametrized by a neural network.

**Notation:** Given a data point  $(y^{(a)}, x, a) \sim p_{Y,X,A}(\cdot)$ , we define  $y_0 = y^{(a)}$  as the observed training sample at time  $t = 0$  in the Neural ODE, and  $y_1 \sim q(\cdot)$  as the noise sample at time  $t = 1$ . Recall that we denote  $\hat{y}^{(a)}$  and  $\hat{y}_{\text{cf}}^{(1-a)}$  as the predicted potential and counterfactual outcomes, respectively.

**Training loss:** PO-Flow adopts the Conditional Flow Matching (CFM) objective for training. Under the updated definitions, our training loss retains the form of Equation (7) and is given by:

$$\min_{\theta} \mathcal{L}_{\text{CFM}}(\theta) = \mathbb{E}_{t \sim \mathcal{U}[0,1], p_{Y,X,A}(\cdot), q(\cdot)} \left\| v_\theta(\phi_t, t, x, a) - \frac{d\phi_t}{dt} \right\|^2, \quad (9)$$

where  $\phi_t$  and  $\frac{d\phi_t}{dt}$  are defined in (5) and (6), respectively.

*Remark:* Following prior work [23, 43], one may estimate propensity scores  $w(x) = p(A = 1 | X = x)$  using a pre-trained classifier and apply inverse probability weighting  $\frac{1}{w(x)}$  in the loss. However, we found this did not improve performance, but both implementations are included in our code.

**Forward Process:** Given the velocity field  $v_\theta$ , the forward process refers to pushing a factual outcome  $y^{(a)}$  (at  $t = 0$ ) to a latent embedding  $z_y$  (at  $t = 1$ ) via:

$$z_y = y^{(a)} + \int_0^1 v_\theta(y(t), t, x, a) dt, \quad \text{with } y(0) = y^{(a)}. \quad (10)$$

Through the forward process,  $z_y$  encodes information from the factual outcome  $y^{(a)}$  as well as its associated covariates  $x$  and treatment  $a$ .

**Reverse Process:** The reverse process is initialized differently for interventional and counterfactual outcome prediction, as detailed in Sections 4.1 and 4.2. In general, given a noise sample  $y_1 \sim q(\cdot)$  at  $t = 1$ , the reverse process is defined as:

$$\hat{y}_0 = y_1 - \int_0^1 v_\theta(y(t), t, x, a) dt, \quad \text{with } y(1) = y_1. \quad (11)$$

Empirically, we use the Runge-Kutta method for numerical integration, with implementation details provided in Appendix B.4.

During training, we construct synthetic paths  $\phi_t$  between  $y_0$  and  $y_1 \sim q(\cdot)$  using the CFM loss, conditioning on  $y_0$ . However, Proposition 4.1 shows that the gradient of the CFM loss with respect to the model parameters is equivalent to the gradient of the original FM loss.

**Proposition 4.1.** Assume that  $p_t(y|x, a) > 0$  for all  $y \in \mathbb{R}^{d_Y}$  and  $t \in [0, 1]$ . Then, up to a constant independent of  $\theta$ , the Conditional Flow Matching (CFM) loss and the original Flow Matching (FM) loss are equivalent. Hence,

$$\nabla_{\theta} \mathcal{L}_{FM}(\theta) = \nabla_{\theta} \mathcal{L}_{CFM}(\theta).$$

As a result of Proposition 4.1, the learned velocity field  $v_{\theta}$  during the reverse process generates samples  $\hat{y}_0$  independent of the individual samples  $y_0$  used during training. Consequently, since  $y_1 \sim q(\cdot)$  is random,  $v_{\theta}$  induces a distribution over outcomes conditioned on  $(x, a)$ .

## 4.1 PO-Flow for Potential Outcomes Prediction

---

### Algorithm 1:

Potential Outcomes Prediction

---

**Require:** Trained  $v_{\theta}$

**Input:**  $(x, a) \sim p_{X,A}(\cdot)$

1:  $y_1 \sim q(\cdot)$

2:  $\hat{y}_0 = y_1 - \int_0^1 v_{\theta}(y(t), t, x, a) dt$

**Return**  $\hat{y}^{(a)} := \hat{y}_0$

---

The potential outcomes prediction in PO-Flow follows a simple reverse process, as defined in Equation (11). Starting from a noise sample  $y_1 \sim q(\cdot)$ , we integrate the velocity field  $v_{\theta}$  backward in time, conditioned on covariates  $x$  and treatment  $a$ , to obtain a point estimate of the potential outcome  $\hat{y}^{(a)}$ . The procedure is summarized in Algorithm 1.

In addition to predicting point estimates of potential outcomes, PO-Flow is capable of learning the probability densities of the potential outcomes, as detailed in Section 4.3.

## 4.2 PO-Flow for Counterfactual Outcomes Prediction

---

### Algorithm 2:

Counterfactual Prediction

---

**Require:** Trained  $v_{\theta}$

**Input:**  $(y^{(a)}, x, a) \sim p_{Y,X,A}(\cdot)$

1. Forward process (encoding):

2.  $z_y = y^{(a)} + \int_0^1 v_{\theta}(y(t), t, x, a) dt,$   
with  $y(0) = y^{(a)}$ .

3. Uncertainty-aware perturbations:

4.  $\delta \sim N(0, \Sigma(x))$

5.  $z'_y = z_y + \delta$

6. Reverse process (decoding):

7.  $\hat{y}_0 = z'_y - \int_0^1 v_{\theta}(y(t), t, x, a) dt,$   
with  $y(1) = z'_y$ .

**Return:**  $\hat{y}_{cf}^{(1-a)} := \hat{y}_0$

---

Under Assumption 3.2, the counterfactual outcome prediction in PO-Flow consists of both a forward and a reverse process. Given a factual observation  $(y^{(a)}, x, a) \sim p_{Y,X,A}(\cdot)$ , the forward process (Lines 2–3 in Algorithm 2) encodes the information  $(y^{(a)}, x, a)$  into a latent representation centered at  $z_y$ . Lines 4–6 introduce uncertainty-aware perturbations to  $z_y$ , reflecting covariate-dependent uncertainty. Finally, the reverse process (Lines 7–8) decodes the latent  $z'_y$  back into the counterfactual outcome prediction  $\hat{y}_{cf}^{(1-a)}$ .

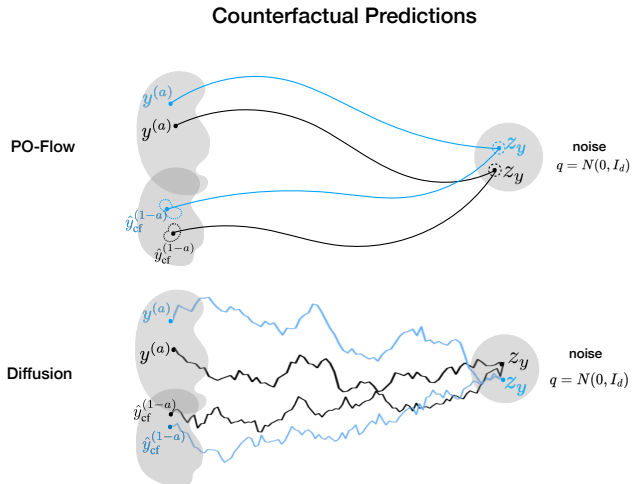


Figure 1: Illustration of counterfactual predictions. *Left*: two potential outcomes distribution. *Right*: Base (noise) distribution.

Because of the smooth and information-preserving nature of the PO-Flow path trained via flow matching, the encoded  $z_y$  retains rich information from the factual outcome  $y^{(a)}$ , enabling accurate decoding of the counterfactual  $\hat{y}_{cf}^{(1-a)}$ . To our knowledge, this is the first work to explore counterfactual outcome prediction using flow or diffusion-based models.

As illustrated in Figure 1, diffusion models rely on noisy and stochastic forward processes, which degrade the information in  $z_y$  and lead to reversed samples that resemble interventional potential outcomes rather than counterfactuals. In Section 5.4, we present counterfactuals using an adapted implementation of DiffPO [43] (originally not designed for counterfactual), compared with PO-Flow.

### 4.3 PO-Flow for Learning Potential Outcomes Densities

Another distinctive advantage of PO-Flow is its ability to learn the density of the Potential Outcomes (POs). We define  $\hat{p}_Y(\cdot | x, a, y_1)$  as the PO density learned by PO-Flow, conditioned on  $(x, a)$  and a base sample  $y_1$ . The explicit form of the learned PO density is presented in Proposition 4.2, with the proof provided in Appendix A.

**Proposition 4.2.** *Given a noise sample  $y_1 \sim q(\cdot)$  at  $t = 1$ , the log-density of the resulting potential outcome at  $t = 0$ , obtained via PO-Flow, is given by:*

$$\log \hat{p}_Y(\cdot | x, a, y_1) = \log q(y_1) + \int_0^1 \nabla \cdot v_\theta(y(t), t, x, a) ds. \quad (12)$$

Empirically, the divergence of the velocity field can be computed under the Hutchinson trace estimator (e.g., [31, 64]). More details are provided in Appendix B.5.

$$\nabla \cdot v_\theta(y(t), t, x, a) \approx \mathbb{E}_{p(\epsilon)} \left[ \epsilon \cdot \frac{v_\theta(y(t) + \sigma\epsilon, t, x, a) - v_\theta(y(t), t, x, a)}{\sigma} \right], \quad (13)$$

where  $p(\epsilon)$  is a distribution in  $\mathbb{R}^{d_Y}$  satisfying  $\mathbb{E}[\epsilon] = 0$  and  $\text{Cov}(\epsilon) = I$  (e.g., a standard Gaussian).

To our knowledge, PO-Flow is the first generative approach in causal inference to explicitly learn the probability density of predicted potential outcomes. Unlike prior works [44, 45] that generate PO samples and estimate empirical distributions, PO-Flow provides direct access to likelihoods, enabling deeper insights into uncertainty.

This density estimation allows PO-Flow to assess prediction confidence via log-likelihood, identify unlikely outcomes, and quantify uncertainty. For counterfactual prediction, one can perturb the latent code  $z'_y$  multiple times and select the most confident  $\hat{y}_{cf}^{(1-a)}$  based on log-likelihood, effectively reducing variance while improving robustness.

## 5 Experiments

*Baselines:* Our baselines cover several categories: model-agnostic learners that learn the conditional distribution means (S-learner and T-learner [37]), representation-based conditional regressors

(Counterfactual Regression (CFR) [55]), generative approaches (Causal Effect Variational Autoencoder (CEVAE) [42]; GAN for Individualized Treatment Effect (GANITE) [67]), and most recent generative approaches based on diffusion (DiffPO [43]) and discrete normalizing flows (INFs [45]).

*Datasets:* Counterfactual outcomes and unobserved potential outcomes (POs) are inaccessible in real-world data but can be simulated in semi-synthetic settings, as discussed in detail in Appendix B.1. Accordingly, we evaluate PO-Flow on standard synthetic benchmarks, including ACIC 2016, ACIC 2018, IHDP, and IBM.

The code and datasets are available at <https://github.com/StatFusion/PO-Flow>.

## 5.1 Prediction of Potential Outcomes

Table 1: Root mean squared error (RMSE) of estimated potential outcomes (POs) across different methods on the ACIC 2018, IHDP, and IBM datasets. Results are averaged over 10-fold cross-validation.

	ACIC 2018		IHDP		IBM	
	RMSE <sub>in</sub>	RMSE <sub>out</sub>	RMSE <sub>in</sub>	RMSE <sub>out</sub>	RMSE <sub>in</sub>	RMSE <sub>out</sub>
<b>PO-Flow</b>	<b>0.53<sub>±.10</sub></b>	0.60 <sub>±.12</sub>	<b>0.98<sub>±.11</sub></b>	<b>1.19<sub>±.13</sub></b>	<b>0.90<sub>±.09</sub></b>	<b>0.97<sub>±.11</sub></b>
DiffPO	0.72 <sub>±.14</sub>	0.79 <sub>±.16</sub>	1.33 <sub>±.20</sub>	1.40 <sub>±.22</sub>	1.82 <sub>±.38</sub>	1.85 <sub>±.35</sub>
INFs	0.69 <sub>±.16</sub>	0.78 <sub>±.17</sub>	1.02 <sub>±.10</sub>	<b>1.20<sub>±.12</sub></b>	1.52 <sub>±.24</sub>	1.57 <sub>±.28</sub>
S-learner	<b>0.54<sub>±.09</sub></b>	<b>0.57<sub>±.11</sub></b>	1.31 <sub>±.18</sub>	1.44 <sub>±.20</sub>	1.01 <sub>±.17</sub>	1.16 <sub>±.19</sub>
T-learner	1.57 <sub>±.32</sub>	1.71 <sub>±.40</sub>	1.45 <sub>±.25</sub>	1.49 <sub>±.27</sub>	1.89 <sub>±.47</sub>	1.96 <sub>±.50</sub>
CEVAE	0.83 <sub>±.17</sub>	0.85 <sub>±.17</sub>	1.18 <sub>±.15</sub>	1.36 <sub>±.18</sub>	0.96 <sub>±.12</sub>	<b>0.98<sub>±.12</sub></b>
CFR	0.94 <sub>±.10</sub>	0.98 <sub>±.12</sub>	1.10 <sub>±.20</sub>	<b>1.18<sub>±.20</sub></b>	2.09 <sub>±.45</sub>	2.17 <sub>±.48</sub>
GANITE	0.88 <sub>±.15</sub>	0.97 <sub>±.15</sub>	1.60 <sub>±.36</sub>	1.67 <sub>±.34</sub>	2.48 <sub>±.39</sub>	2.59 <sub>±.47</sub>

*Evaluation Metrics:* We evaluate the point estimates of potential outcomes (POs) using the root mean squared error (RMSE) between the estimated outcomes  $\hat{y}_i$  and the true outcomes  $y_i$ , computed as  $\text{RMSE} = \sqrt{\frac{1}{n} \sum_{i=1}^n (y_i - \hat{y}_i)^2}$ . RMSE<sub>in</sub> and RMSE<sub>out</sub> refer to the RMSE evaluated on the training and test sets, respectively.

*Results:* Table 1 shows that PO-Flow achieves the most accurate prediction of potential outcomes on the majority of datasets.

## 5.2 Estimation of CATEs

*Conditional Average Treatment Effect (CATE):* The CATE is defined as  $\tau(x) = \mathbb{E}[y_1 - y_0 \mid X = x]$ , representing the expected treatment effect conditioned on covariates  $x$ . It captures individual-level heterogeneity in causal effects.

*Evaluation Metrics:* We evaluate CATE using the precision in estimation of heterogeneous effect (PEHE), defined as the mean squared error between estimated and true effects:  $\epsilon_{\text{PEHE}} = \frac{1}{n} \sum_{i=1}^n (\hat{\tau}(x_i) - \tau(x_i))^2$ . Table 5 reports the root PEHE for both training and test sets. PO-Flow achieves the most accurate CATE estimates on most datasets.

Table 2: Root Precision in Estimation of Heterogeneous Effect ( $\sqrt{\epsilon_{\text{PEHE}}}$ ) across different methods on the ACIC 2016, ACIC 2018, IHDP, and IBM datasets. Results are averaged over 10-fold cross-validation.

	ACIC 2016		ACIC 2018		IHDP		IBM	
	$\sqrt{\epsilon_{\text{PEHE}}^{\text{in}}}$	$\sqrt{\epsilon_{\text{PEHE}}^{\text{out}}}$	$\sqrt{\epsilon_{\text{PEHE}}^{\text{in}}}$	$\sqrt{\epsilon_{\text{PEHE}}^{\text{out}}}$	$\sqrt{\epsilon_{\text{PEHE}}^{\text{in}}}$	$\sqrt{\epsilon_{\text{PEHE}}^{\text{out}}}$	$\sqrt{\epsilon_{\text{PEHE}}^{\text{in}}}$	$\sqrt{\epsilon_{\text{PEHE}}^{\text{out}}}$
<b>PO-Flow</b>	<b>0.76<sub>±.08</sub></b>	<b>0.82<sub>±.09</sub></b>	<b>0.05<sub>±.01</sub></b>	<b>0.07<sub>±.02</sub></b>	<b>0.41<sub>±.08</sub></b>	<b>0.45<sub>±.10</sub></b>	<b>0.04<sub>±.01</sub></b>	<b>0.04<sub>±.01</sub></b>
DiffPO	0.91 <sub>±.20</sub>	1.12 <sub>±.26</sub>	0.07 <sub>±.03</sub>	<b>0.08<sub>±.04</sub></b>	0.79 <sub>±.16</sub>	0.84 <sub>±.18</sub>	0.08 <sub>±.03</sub>	0.09 <sub>±.03</sub>
INFs	1.37 <sub>±.28</sub>	1.42 <sub>±.30</sub>	0.33 <sub>±.11</sub>	0.37 <sub>±.12</sub>	0.90 <sub>±.27</sub>	0.95 <sub>±.27</sub>	0.16 <sub>±.08</sub>	0.18 <sub>±.08</sub>
S-learner	3.81 <sub>±.76</sub>	3.87 <sub>±.98</sub>	<b>0.06<sub>±.02</sub></b>	<b>0.07<sub>±.03</sub></b>	0.92 <sub>±.07</sub>	0.93 <sub>±.08</sub>	0.06 <sub>±.02</sub>	0.07 <sub>±.04</sub>
T-learner	5.02 <sub>±.71</sub>	5.15 <sub>±.87</sub>	1.21 <sub>±.47</sub>	1.32 <sub>±.53</sub>	1.24 <sub>±.08</sub>	1.31 <sub>±.09</sub>	0.60 <sub>±.14</sub>	0.69 <sub>±.15</sub>
CEVAE	2.06 <sub>±.61</sub>	2.31 <sub>±.74</sub>	1.19 <sub>±.15</sub>	1.21 <sub>±.16</sub>	1.41 <sub>±.10</sub>	1.43 <sub>±.10</sub>	0.73 <sub>±.15</sub>	0.75 <sub>±.16</sub>
CFR	2.80 <sub>±.58</sub>	2.74 <sub>±.60</sub>	0.77 <sub>±.18</sub>	0.80 <sub>±.18</sub>	<b>0.73<sub>±.04</sub></b>	0.78 <sub>±.04</sub>	1.05 <sub>±.27</sub>	1.08 <sub>±.28</sub>
GANITE	3.02 <sub>±.76</sub>	3.11 <sub>±.74</sub>	0.55 <sub>±.11</sub>	0.60 <sub>±.13</sub>	1.90 <sub>±.40</sub>	2.40 <sub>±.40</sub>	0.77 <sub>±.20</sub>	0.80 <sub>±.24</sub>

### 5.3 Learning the Full Potential Outcome Distributions

Beyond point estimation, PO-Flow offers two distinct advantages for modeling potential outcomes: (1) it enables individualized sampling from the conditional distribution  $P(Y | X, A)$ , generating a rich set of plausible outcomes for each individual; and (2) it supports learning the probability density of any generated outcome, providing deeper insights into predictive uncertainty.

#### 5.3.1 Learning potential outcome densities

PO-Flow enables direct computation of potential outcome densities, as shown in Proposition 4.2. To our knowledge, it is the first generative method in causal potential outcomes to provide this capability.

*Evaluation Metrics:* To evaluate the learned densities, we compute the KL divergence between the PO-Flow estimate  $\hat{p}(\cdot|x, a)$  and the ground-truth density  $p_{\text{true}}(\cdot|x, a)$ . Given that the semi-synthetic datasets assume  $y^{(a)} \sim \mathcal{N}(\mu(a), 1)$ , the individual-level KL is  $\text{KL}(\hat{Y}_X^{(a)} \| Y_X^{(a)}) = \mathbb{E}_{\hat{y} \sim \hat{p}} \left[ \log \frac{\hat{p}(\hat{y}|x, a)}{\mathcal{N}(\mu(\hat{y}), 1)} \right]$ , where  $\hat{p}$  is computed via (12). Table 3 reports the average results.

Table 3: KL divergence of learned potential outcome distributions across datasets. Results are averaged over 10-fold cross-validation.

	ACIC 2016	ACIC 2018	IHDP	IBM
PO-Flow	0.14 $\pm$ .04	0.08 $\pm$ .02	0.09 $\pm$ .03	0.08 $\pm$ .03
GP-ITE	1.73 $\pm$ .34	0.73 $\pm$ .19	1.42 $\pm$ .30	0.68 $\pm$ .17

*Baselines:* A natural baseline with density estimation capability is Gaussian Processes for interventional treatment effects, as used in [3, 30].

*Results:* PO-Flow achieves much lower KL divergence than GP baselines on the ACIC 2018, IHDP, and IBM datasets, indicating more accurate density estimation of potential outcomes.

This property allows PO-Flow to assess prediction confidence via log-density and to identify unlikely outcomes. For counterfactual estimation, one can sample multiple candidates from a perturbed latent region and select the most likely one based on the model’s estimated density.

#### 5.3.2 Empirical distribution estimations

*Evaluation Metrics:* To enable comparison of estimated potential outcome distributions across methods, we include empirical distribution estimates for all baselines. These are evaluated using the Wasserstein-1 distance, defined as:  $W_1(\hat{p}(y|x, a), p(y|x, a)) = \inf_{\gamma \in \Gamma(\hat{p}, p)} \mathbb{E}_{(\hat{y}, y \sim \gamma)} [\|\hat{y} - y\|_1]$ . The results are shown in Table 4.

Table 4: In-sample and out-of-sample Wasserstein distances across different methods on the ACIC 2016, ACIC 2018, IHDP, and IBM datasets. Results are averaged over 10-fold cross-validation.

	ACIC 2016		ACIC 2018		IHDP		IBM	
	$\hat{W}_1^{\text{in}}$	$\hat{W}_1^{\text{out}}$	$\hat{W}_1^{\text{in}}$	$\hat{W}_1^{\text{out}}$	$\hat{W}_1^{\text{in}}$	$\hat{W}_1^{\text{out}}$	$\hat{W}_1^{\text{in}}$	$\hat{W}_1^{\text{out}}$
PO-Flow	0.36 $\pm$ .11	0.42 $\pm$ .12	0.05 $\pm$ .03	0.12 $\pm$ .04	0.30 $\pm$ .05	0.41 $\pm$ .06	0.33 $\pm$ .07	0.44 $\pm$ .08
DiffPO	0.47 $\pm$ .17	0.51 $\pm$ .18	0.04 $\pm$ .02	0.13 $\pm$ .05	0.80 $\pm$ .15	0.88 $\pm$ .17	0.69 $\pm$ .14	0.75 $\pm$ .14
INFs	0.59 $\pm$ .13	0.67 $\pm$ .14	0.08 $\pm$ .03	0.16 $\pm$ .05	0.32 $\pm$ .08	0.40 $\pm$ .09	0.36 $\pm$ .08	0.45 $\pm$ .09
S-learner	1.01 $\pm$ .13	1.02 $\pm$ .20	0.35 $\pm$ .13	0.49 $\pm$ .20	0.71 $\pm$ .14	0.85 $\pm$ .19	0.46 $\pm$ .11	0.55 $\pm$ .14
T-learner	1.22 $\pm$ .15	1.48 $\pm$ .18	1.04 $\pm$ .13	1.00 $\pm$ .30	0.83 $\pm$ .20	0.92 $\pm$ .28	1.21 $\pm$ .23	1.67 $\pm$ .32
CEVAE	0.62 $\pm$ .17	0.70 $\pm$ .21	0.88 $\pm$ .18	1.02 $\pm$ .23	0.65 $\pm$ .14	0.76 $\pm$ .20	0.38 $\pm$ .07	0.45 $\pm$ .07
CFR	0.68 $\pm$ .13	0.73 $\pm$ .15	0.88 $\pm$ .12	0.90 $\pm$ .15	0.50 $\pm$ .17	0.56 $\pm$ .19	0.92 $\pm$ .20	0.93 $\pm$ .21
GANITE	0.74 $\pm$ .20	0.86 $\pm$ .23	0.89 $\pm$ .24	1.18 $\pm$ .25	0.71 $\pm$ .23	0.82 $\pm$ .29	1.09 $\pm$ .27	1.34 $\pm$ .30

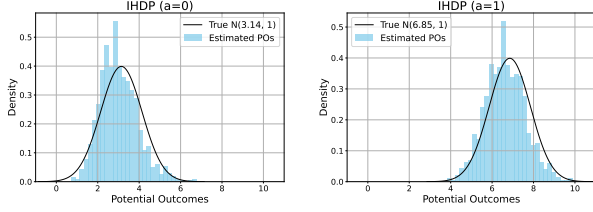


Figure 2: Comparison between empirically estimated and the ground-truth POs distributions. Left:  $P(y|x, a = 0)$  on IHDP. Right:  $P(y|x, a = 1)$  on IHDP.

Understanding the distribution of potential outcomes (POs) is essential for reasoning about uncertainty in treatment decisions. As shown in Figure 2, PO distributions can shift differently across treatments for the same individual. PO-Flow provides not only point estimates but also distributional insight, supporting uncertainty-aware analysis. Section 5.3.1 further demonstrates its ability to estimate densities accurately. This enables practitioners to assess whether an outcome lies within a desired range and evaluate its likelihood (Proposition 4.2) under a given treatment, offering a clearer sense of confidence in the effect.

## 5.4 Counterfactual Outcome Estimation

*Evaluation Metrics:* We evaluate the predicted counterfactual outcomes using the root mean squared error (RMSE) between the estimated counterfactuals  $\hat{y}_{i,cf}^{(1-a)}$  and the ground-truth counterfactuals  $y_{i,cf}^{(1-a)}$ , computed as  $RMSE = \sqrt{\frac{1}{n} \sum_{i=1}^n (y_{i,cf}^{(1-a)} - \hat{y}_{i,cf}^{(1-a)})^2}$ . The results are presented in Table 5. Here,  $RMSE_{in}$  and  $RMSE_{out}$  denote the RMSE evaluated on the training and test sets, respectively.

*Baselines:* To our knowledge, very few existing methods are specifically designed for counterfactual outcome prediction conditioned on factuials in general settings—without relying on structural causal models or temporal information. While methods like CFR include “counterfactual” in name, they target unobserved potential outcomes rather than factual-conditioned ones, though we still include them as valuable baselines. We also adapt DiffPO and GANITE for this task, as detailed in Appendix B.6.

Table 5: Root mean squared error (RMSE) of estimated counterfactual outcomes across different methods on the ACIC 2016, ACIC 2018, IHDP, and IBM datasets. Results are averaged over 10-fold cross-validation.

	ACIC 2016		ACIC 2018		IHDP		IBM	
	RMSE <sub>in</sub>	RMSE <sub>out</sub>						
<b>PO-Flow</b>	<b>1.50<sub>±.15</sub></b>	<b>1.53<sub>±.17</sub></b>	<b>0.04<sub>±.01</sub></b>	<b>0.05<sub>±.02</sub></b>	<b>1.63<sub>±.09</sub></b>	1.69 <sub>±.10</sub>	<b>0.04<sub>±.01</sub></b>	<b>0.04<sub>±.02</sub></b>
DiffPO	1.77 <sub>±.20</sub>	1.78 <sub>±.20</sub>	0.62 <sub>±.14</sub>	0.65 <sub>±.15</sub>	1.81 <sub>±.22</sub>	1.85 <sub>±.23</sub>	0.62 <sub>±.13</sub>	0.64 <sub>±.16</sub>
CFR	3.15 <sub>±.28</sub>	3.38 <sub>±.30</sub>	0.99 <sub>±.05</sub>	1.01 <sub>±.07</sub>	<b>1.63<sub>±.21</sub></b>	<b>1.65<sub>±.25</sub></b>	0.86 <sub>±.18</sub>	0.87 <sub>±.16</sub>
GANITE	3.41 <sub>±.52</sub>	3.67 <sub>±.55</sub>	0.68 <sub>±.13</sub>	0.70 <sub>±.14</sub>	2.48 <sub>±.53</sub>	2.72 <sub>±.59</sub>	1.84 <sub>±.30</sub>	2.02 <sub>±.37</sub>

## 5.5 Counterfactual Image Generation

Beyond low-dimensional datasets, PO-Flow also succeeds on high-dimensional counterfactual image generation. We train PO-Flow on the latent space of a pre-trained VAE using the CelebA dataset, predicting counterfactual male faces from original female faces. In this setting,  $X \in \mathbb{R}^6$  encodes visual attributes (hair, eyebrows, bangs, lips),  $a \in \{\text{male, female}\}$  denotes gender, and  $y \in \mathbb{R}^{512}$  is the VAE latent feature. Visual results are shown in Figures 3 and 5; detailed settings are in Appendix B.2.

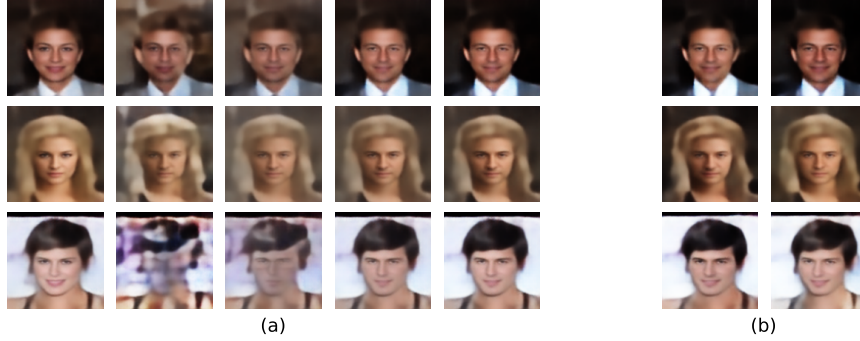


Figure 3: PO-Flow counterfactual image generation from female to male faces. (a): Each row shows a factual outcome  $y^{(a)}$  (1st column), its encoded latent  $z_y$  (2nd column), and reverse-time decoding at  $t = 2/3$ ,  $t = 1/3$ , and  $t = 0$  (3rd–5th columns), yielding the counterfactual  $\hat{y}_{\text{cf}}^{(1-a)}$ . (b): Counterfactuals decoded from perturbed latents  $z_y + \delta$ , with  $\delta \sim \mathcal{N}(0, 0.2I)$ .

## 5.6 Discussions and Comparisons

*Training efficiency:* PO-Flow exhibits high training efficiency, converging in approximately 300 gradient steps across multiple causal datasets, as shown in Appendix C.1.

*Minimal architecture sensitivity:* We find that PO-Flow is the least sensitive to neural network architecture and hyperparameters. Using the same NN structure across all causal datasets, PO-Flow consistently achieves state-of-the-art performance. In contrast, we find that generative approaches including DiffPO, INFs, and GANITE require careful hyperparameter tuning for each dataset.

*Unique density estimation:* Our continuous normalizing flow (CNF) backbone enables density learning of potential outcomes, as shown in Proposition 4.2 and Section 5.3.1, which, to our knowledge, is the first generative model in the field to achieve this.

*Counterfactual:* We take a step further by exploring counterfactual outcomes, enabled by the smooth PO-Flow mapping that preserves factual information during encoding. Unlike diffusion-based DiffPO, which has noisy forward processes, PO-Flow offers information-preserving forward processes, as shown in Figure 1. To our knowledge, it is among the first to explore empirical counterfactual prediction without relying on temporal data or explicitly modeling structural causal models.

However, one area for improving counterfactual prediction lies in modeling uncertainty more expressively. The current covariate-conditioned Gaussian perturbations may not fully capture counterfactual variation. Future work could explore more theoretically grounded counterfactual uncertainty.

## 6 Conclusions

We introduced PO-Flow, a continuous normalizing flow framework for modeling potential and counterfactual outcomes in causal inference. PO-Flow provides a unified generative framework for potential outcome prediction, CATE estimation, and general-purpose counterfactual prediction—without explicitly modeling structural causal models (SCMs) or relying on auxiliary information for the counterfactual task.

Empirically, PO-Flow achieves state-of-the-art performance on benchmark datasets across multiple causal tasks. Among generative models, it is the first to accurately learn the density of potential outcomes, enabling principled uncertainty quantification. Furthermore, PO-Flow is efficient, robust,

and extendable to high-dimensional settings such as counterfactual image generation. These results highlight PO-Flow as a unified and scalable solution for causal inference tasks.

## Acknowledgment

D.I. acknowledges support from NSF (IIS-2212097), ARL (W911NF-2020-221), and ONR (N00014-23-C-1016). Y.X. acknowledges partial support from NSF DMS-2134037, CMMI-2112533, and the Coca-Cola Foundation. Any opinions, findings, and conclusions or recommendations expressed in this material are those of the authors and do not necessarily reflect the views of the sponsor(s).

## References

- [1] Jason Abrevaya, Yu-Chin Hsu, and Robert P Lieli. Estimating conditional average treatment effects. *Journal of Business & Economic Statistics*, 33(4):485–505, 2015.
- [2] Naoufal Acharki, Ramiro Lugo, Antoine Bertonecello, and Josselin Garnier. Comparison of meta-learners for estimating multi-valued treatment heterogeneous effects. In *International conference on machine learning*, pages 91–132. PMLR, 2023.
- [3] Ahmed M Alaa and Mihaela Van Der Schaar. Bayesian inference of individualized treatment effects using multi-task gaussian processes. *Advances in neural information processing systems*, 30, 2017.
- [4] Michael S Albergo and Eric Vanden-Eijnden. Building normalizing flows with stochastic interpolants. *arXiv preprint arXiv:2209.15571*, 2022.
- [5] Ioana Bica, Ahmed M Alaa, James Jordon, and Mihaela van der Schaar. Estimating counterfactual treatment outcomes over time through adversarially balanced representations. *arXiv preprint arXiv:2002.04083*, 2020.
- [6] Tineke Blom, Stephan Bongers, and Joris M Mooij. Beyond structural causal models: Causal constraints models. In *Uncertainty in Artificial Intelligence*, pages 585–594. PMLR, 2020.
- [7] Stephan Bongers, Patrick Forré, Jonas Peters, and Joris M Mooij. Foundations of structural causal models with cycles and latent variables. *The Annals of Statistics*, 49(5):2885–2915, 2021.
- [8] Gert-Jan Both and Remy Kusters. Temporal normalizing flows. *arXiv preprint arXiv:1912.09092*, 2019.
- [9] Patrick Chao, Patrick Blöbaum, and Shiva Prasad Kasiviswanathan. Interventional and counterfactual inference with diffusion models. *arXiv preprint arXiv:2302.00860*, 4:16, 2023.
- [10] Patrick Chao, Patrick Blöbaum, Sapan Patel, and Shiva Prasad Kasiviswanathan. Modeling causal mechanisms with diffusion models for interventional and counterfactual queries. *arXiv preprint arXiv:2302.00860*, 2023.
- [11] Arthur Charpentier, Emmanuel Flachaire, and Ewen Gallic. Optimal transport for counterfactual estimation: A method for causal inference. In *Optimal Transport Statistics for Economics and Related Topics*, pages 45–89. Springer, 2023.

- [12] Ricky TQ Chen, Yulia Rubanova, Jesse Bettencourt, and David K Duvenaud. Neural ordinary differential equations. *Advances in neural information processing systems*, 31, 2018.
- [13] Yuansi Chen and Peter Bühlmann. Domain adaptation under structural causal models. *Journal of Machine Learning Research*, 22(261):1–80, 2021.
- [14] Hugh A Chipman, Edward I George, and Robert E McCulloch. Bart: Bayesian additive regression trees. 2010.
- [15] Alicia Curth and Mihaela Van der Schaar. Nonparametric estimation of heterogeneous treatment effects: From theory to learning algorithms. In *International Conference on Artificial Intelligence and Statistics*, pages 1810–1818. PMLR, 2021.
- [16] Alicia Curth and Mihaela Van der Schaar. On inductive biases for heterogeneous treatment effect estimation. *Advances in Neural Information Processing Systems*, 34:15883–15894, 2021.
- [17] Lucas De Lara, Alberto González-Sanz, Nicholas Asher, Laurent Risser, and Jean-Michel Loubes. Transport-based counterfactual models. *Journal of Machine Learning Research*, 25(136):1–59, 2024.
- [18] Mingzhou Fan, Ruida Zhou, Chao Tian, and Xiaoning Qian. Path-guided particle-based sampling. *arXiv preprint arXiv:2412.03312*, 2024.
- [19] Karim Farid, Simon Schrodi, Max Argus, and Thomas Brox. Latent diffusion counterfactual explanations. *arXiv preprint arXiv:2310.06668*, 2023.
- [20] Stefan Feuerriegel, Dennis Frauen, Valentyn Melnychuk, Jonas Schweisthal, Konstantin Hess, Alicia Curth, Stefan Bauer, Niki Kilbertus, Isaac S Kohane, and Mihaela van der Schaar. Causal machine learning for predicting treatment outcomes. *Nature Medicine*, 30(4):958–968, 2024.
- [21] Riccardo Guidotti. Counterfactual explanations and how to find them: literature review and benchmarking. *Data Mining and Knowledge Discovery*, 38(5):2770–2824, 2024.
- [22] P Richard Hahn, Jared S Murray, and Carlos M Carvalho. Bayesian regression tree models for causal inference: Regularization, confounding, and heterogeneous effects (with discussion). *Bayesian Analysis*, 15(3):965–1056, 2020.
- [23] Jason S Haukoos and Roger J Lewis. The propensity score. *Jama*, 314(15):1637–1638, 2015.
- [24] Jennifer L Hill. Bayesian nonparametric modeling for causal inference. *Journal of Computational and Graphical Statistics*, 20(1):217–240, 2011.
- [25] Keisuke Hirano, Guido W Imbens, and Geert Ridder. Efficient estimation of average treatment effects using the estimated propensity score. *Econometrica*, 71(4):1161–1189, 2003.
- [26] Jonathan Ho, Ajay Jain, and Pieter Abbeel. Denoising diffusion probabilistic models. *Advances in neural information processing systems*, 33:6840–6851, 2020.
- [27] Marc Höfler. Causal inference based on counterfactuals. *BMC medical research methodology*, 5:1–12, 2005.
- [28] Paul W Holland. Statistics and causal inference. *Journal of the American statistical Association*, 81(396):945–960, 1986.

- [29] Yu-Chin Hsu, Tsung-Chih Lai, and Robert P Lieli. Counterfactual treatment effects: Estimation and inference. *Journal of Business & Economic Statistics*, 40(1):240–255, 2022.
- [30] Bin Huang, Chen Chen, Jinzhong Liu, and Siva Sivaganisan. Gpmatch: A bayesian causal inference approach using gaussian process covariance function as a matching tool. *Frontiers in Applied Mathematics and Statistics*, 9:1122114, 2023.
- [31] Michael F Hutchinson. A stochastic estimator of the trace of the influence matrix for laplacian smoothing splines. *Communications in Statistics-Simulation and Computation*, 18(3):1059–1076, 1989.
- [32] Guido W Imbens. Nonparametric estimation of average treatment effects under exogeneity: A review. *Review of Economics and statistics*, 86(1):4–29, 2004.
- [33] Adrián Javaloy, Pablo Sánchez-Martín, and Isabel Valera. Causal normalizing flows: from theory to practice. *Advances in Neural Information Processing Systems*, 36:58833–58864, 2023.
- [34] Fredrik Johansson, Uri Shalit, and David Sontag. Learning representations for counterfactual inference. In *International conference on machine learning*, pages 3020–3029. PMLR, 2016.
- [35] Fredrik D Johansson, Uri Shalit, Nathan Kallus, and David Sontag. Generalization bounds and representation learning for estimation of potential outcomes and causal effects. *Journal of Machine Learning Research*, 23(166):1–50, 2022.
- [36] Diederik P Kingma, Max Welling, et al. Auto-encoding variational bayes, 2013.
- [37] Sören R Künzle, Jasjeet S Sekhon, Peter J Bickel, and Bin Yu. Metalearners for estimating heterogeneous treatment effects using machine learning. *Proceedings of the national academy of sciences*, 116(10):4156–4165, 2019.
- [38] Lihua Lei and Emmanuel J Candès. Conformal inference of counterfactuals and individual treatment effects. *Journal of the Royal Statistical Society Series B: Statistical Methodology*, 83(5):911–938, 2021.
- [39] Rui Li, Zach Shahn, Jun Li, Mingyu Lu, Prithwish Chakraborty, Daby Sow, Mohamed Ghalwash, and Li-wei H Lehman. G-net: a deep learning approach to g-computation for counterfactual outcome prediction under dynamic treatment regimes. *arXiv preprint arXiv:2003.10551*, 2020.
- [40] Yaron Lipman, Ricky T. Q. Chen, Heli Ben-Hamu, Maximilian Nickel, and Matt Le. Flow matching for generative modeling. In *International Conference on Learning Representations (ICLR)*, 2023.
- [41] Roderick J Little and Donald B Rubin. Causal effects in clinical and epidemiological studies via potential outcomes: concepts and analytical approaches. *Annual review of public health*, 21(1):121–145, 2000.
- [42] Christos Louizos, Uri Shalit, Joris M Mooij, David Sontag, Richard Zemel, and Max Welling. Causal effect inference with deep latent-variable models. *Advances in neural information processing systems*, 30, 2017.
- [43] Yuchen Ma, Qingshuo Wang, Jiayu Xu, Jiaming Zhang, Zekun Xu, Siliang Li, and Zhanxing Liu. Diffpo: A causal diffusion model for learning distributions of potential outcomes. In *Proceedings of the 38th Annual Conference on Neural Information Processing Systems (NeurIPS)*, 2024.

- [44] Valentyn Melnychuk, Dennis Frauen, and Stefan Feuerriegel. Causal transformer for estimating counterfactual outcomes. In *International conference on machine learning*, pages 15293–15329. PMLR, 2022.
- [45] Valentyn Melnychuk, Dennis Frauen, and Stefan Feuerriegel. Normalizing flows for interventional density estimation. In *International Conference on Machine Learning*, pages 24361–24397. PMLR, 2023.
- [46] Joris M Mooij, Dominik Janzing, and Bernhard Schölkopf. From ordinary differential equations to structural causal models: the deterministic case. *arXiv preprint arXiv:1304.7920*, 2013.
- [47] Arash Nasr-Esfahany and Emre Kiciman. Counterfactual (non-) identifiability of learned structural causal models. *arXiv preprint arXiv:2301.09031*, 2023.
- [48] Leland Gerson Neuberger. Causality: models, reasoning, and inference, by judea pearl, cambridge university press, 2000. *Econometric Theory*, 19(4):675–685, 2003.
- [49] Nick Pawlowski, Daniel Coelho de Castro, and Ben Glocker. Deep structural causal models for tractable counterfactual inference. *Advances in neural information processing systems*, 33:857–869, 2020.
- [50] Mattia Prosperi, Yi Guo, Matt Sperrin, James S Koopman, Jae S Min, Xing He, Shannan Rich, Mo Wang, Iain E Buchan, and Jiang Bian. Causal inference and counterfactual prediction in machine learning for actionable healthcare. *Nature Machine Intelligence*, 2(7):369–375, 2020.
- [51] Chengping Rao, Pu Ren, Qi Wang, Oral Buyukozturk, Hao Sun, and Yang Liu. Encoding physics to learn reaction–diffusion processes. *Nature Machine Intelligence*, 5(7):765–779, 2023.
- [52] Donald B Rubin. Causal inference using potential outcomes: Design, modeling, decisions. *Journal of the American statistical Association*, 100(469):322–331, 2005.
- [53] Pedro Sanchez and Sotirios A Tsafaris. Diffusion causal models for counterfactual estimation. *arXiv preprint arXiv:2202.10166*, 2022.
- [54] Jonas Schweisthal, Dennis Frauen, Mihaela Van Der Schaar, and Stefan Feuerriegel. Meta-learners for partially-identified treatment effects across multiple environments. In *Forty-first International Conference on Machine Learning*, 2024.
- [55] Uri Shalit, Fredrik D Johansson, and David Sontag. Estimating individual treatment effect: generalization bounds and algorithms. In *International conference on machine learning*, pages 3076–3085. PMLR, 2017.
- [56] Yishai Shimoni, Chen Yanover, Ehud Karavani, and Yaara Goldschmndt. Benchmarking framework for performance-evaluation of causal inference analysis. *arXiv preprint arXiv:1802.05046*, 2018.
- [57] Jiaming Song, Chenlin Meng, and Stefano Ermon. Denoising diffusion implicit models. *arXiv preprint arXiv:2010.02502*, 2020.
- [58] Yang Song, Prafulla Dhariwal, Mark Chen, and Ilya Sutskever. Consistency models. 2023.
- [59] Yifeng Tian, Nishant Panda, and Yen Ting Lin. Liouville flow importance sampler. *arXiv preprint arXiv:2405.06672*, 2024.

- [60] Marc K Walton, John H Powers III, Jeremy Hobart, Donald Patrick, Patrick Marquis, Spiros Vamvakas, Maria Isaac, Elizabeth Molsen, Stefan Cano, and Laurie B Burke. Clinical outcome assessments: conceptual foundation—report of the ispor clinical outcomes assessment—emerging good practices for outcomes research task force. *Value in Health*, 18(6):741–752, 2015.
- [61] Dongze Wu and Yao Xie. Annealing flow generative model towards sampling high-dimensional and multi-modal distributions. *arXiv preprint arXiv:2409.20547*, 2024.
- [62] Shenghao Wu, Wenbin Zhou, Minshuo Chen, and Shixiang Zhu. Counterfactual generative models for time-varying treatments. In *Proceedings of the 30th ACM SIGKDD Conference on Knowledge Discovery and Data Mining*, pages 3402–3413, 2024.
- [63] Yongkai Wu, Lu Zhang, and Xintao Wu. Counterfactual fairness: Unidentification, bound and algorithm. In *Proceedings of the twenty-eighth international joint conference on Artificial Intelligence*, 2019.
- [64] Chen Xu, Xiuyuan Cheng, and Yao Xie. Normalizing flow neural networks by jko scheme. *Advances in Neural Information Processing Systems*, 36:47379–47405, 2023.
- [65] Mengyue Yang, Furui Liu, Zhitang Chen, Xinwei Shen, Jianye Hao, and Jun Wang. Causalvae: Disentangled representation learning via neural structural causal models. In *Proceedings of the IEEE/CVF conference on computer vision and pattern recognition*, pages 9593–9602, 2021.
- [66] Zhen Yang, Yongbin Liu, Chunping Ouyang, Lin Ren, and Wen Wen. Counterfactual can be strong in medical question and answering. *Information Processing & Management*, 60(4):103408, 2023.
- [67] Jinsung Yoon, James Jordon, and Mihaela Van Der Schaar. Ganite: Estimation of individualized treatment effects using generative adversarial nets. In *International conference on learning representations*, 2018.
- [68] Ye Yuan, Jiaming Song, Umar Iqbal, Arash Vahdat, and Jan Kautz. Physdiff: Physics-guided human motion diffusion model. In *Proceedings of the IEEE/CVF international conference on computer vision*, pages 16010–16021, 2023.
- [69] Zhiwei Zhang, Chenguang Wang, Lei Nie, and Guoxing Soon. Assessing the heterogeneity of treatment effects via potential outcomes of individual patients. *Journal of the Royal Statistical Society Series C: Applied Statistics*, 62(5):687–704, 2013.
- [70] Zeyu Zhou, Ruqi Bai, Sean Kulinski, Murat Kocaoglu, and David I Inouye. Towards characterizing domain counterfactuals for invertible latent causal models. *arXiv preprint arXiv:2306.11281*, 2023.

## A Proofs

**Proposition 4.1.** *Assume that  $p_t(y|x, a) > 0$  for all  $y \in \mathbb{R}^{d_Y}$  and  $t \in [0, 1]$ . Then, up to a constant independent of  $\theta$ , the Conditional Flow Matching (CFM) loss and the original Flow Matching (FM) loss are equivalent. Hence,*

$$\nabla_{\theta} \mathcal{L}_{FM}(\theta) = \nabla_{\theta} \mathcal{L}_{CFM}(\theta).$$

*Proof:*

We denote the conditional reference velocity field as  $u(y, t, x, a|y_0) = \frac{d\phi_t}{dt} = (1 - \sigma_{\min})y_1 - y_0$ , as defined in (6). We further define the marginal (unconditional) reference velocity field as:

$$u(y, t, x, a) = \int u(y, t, x, a|y_0) \frac{p(y, t, x, a|y_0)p_Y(y_0)}{p(y, t, x, a)} dy_0, \quad (14)$$

where  $p(y, t, x, a|y_0)$  and  $p(y, t, x, a)$  denote the probability densities induced by  $u(y, t, x, a|y_0)$  and  $u(y, t, x, a)$ , respectively. Next, the original flow matching loss, unconditioned on  $y_0$ , is defined as:

$$\mathcal{L}_{FM} = \mathbb{E}_{t \sim \mathcal{U}[0,1], p_{Y_t, X, A}(\cdot)} \|v_{\theta}(y_t, t, x, a) - u(y_t, t, x, a)\|^2. \quad (15)$$

In the main text, we chose  $\phi_t$  as the linear interpolant between  $y_0$  and  $y_1$ , which results in a constant reference velocity  $\frac{d\phi_t}{dt}$  independent of  $t$ . This leads to the simplified CFM loss presented in Eq. (9). However, the general CFM loss, corresponding to an arbitrary reference velocity field  $u(y, t | y_0)$  conditioned on  $y_0$ , is defined as:

$$\mathcal{L}_{CFM} = \mathbb{E}_{t \sim \mathcal{U}[0,1], p_Y(y_0), p_{Y_t, X, A|Y_0}(\cdot|y_0)} \|v_{\theta}(\cdot) - u_t(\cdot|y_0)\|^2 \quad (16)$$

Next, we have that:

$$\begin{aligned} \|v_{\theta}(y, t, x, a) - u(y, t, x, a)\|^2 &= \|v_{\theta}(\cdot)\|^2 - 2\langle v_{\theta}(\cdot), u(\cdot) \rangle + \|u(\cdot)\|^2 \\ \|v_{\theta}(y, t, x, a) - u(y, t, x, a|y_0)\|^2 &= \|v_{\theta}(\cdot)\|^2 - 2\langle v_{\theta}(\cdot), u(\cdot|y_0) \rangle + \|u(\cdot|y_0)\|^2. \end{aligned} \quad (17)$$

Besides, the term  $\mathbb{E}_{t \sim \mathcal{U}[0,1], p_{Y_t, X, A}(\cdot)} \|v_{\theta}(\cdot)\|^2$  can be equivalently expressed in conditional form as:

$$\begin{aligned} \mathbb{E}_{t \sim \mathcal{U}[0,1], p_{Y_t, X, A}(\cdot)} \|v_{\theta}(\cdot)\|^2 &= \int \|v_{\theta}(\cdot)\|^2 p_{Y_t, X, A}(\cdot) dy dx da dt \\ &= \int \|v_{\theta}(\cdot)\|^2 p_{Y_t, X, A|Y_0}(\cdot|y_0) p_Y(y_0) dy_0 dy dx da dt \\ &= \mathbb{E}_{t \sim \mathcal{U}[0,1], p_Y(y_0), p_{Y_t, X, A|Y_0}(\cdot|y_0)} \|v_{\theta}(\cdot)\|^2. \end{aligned} \quad (18)$$

Furthermore, by the law of total expectation, we have:

$$\begin{aligned} \mathbb{E}_{t \sim \mathcal{U}[0,1], p_{Y_t, X, A}(\cdot)} \langle v_{\theta}(\cdot), u(\cdot) \rangle &= \int \left\langle v_{\theta}(\cdot), \frac{\int u(\cdot|y_0) p_{Y_t, X, A}(\cdot|y_0) p_Y(y_0) dy_0}{p_{Y_t, X, A}(\cdot)} \right\rangle p_{Y_t, X, A}(\cdot) dy dx da dt \\ &= \int \left\langle v_{\theta}(\cdot), \int u(\cdot|y_0) p_{Y_t, X, A}(\cdot|y_0) p_Y(y_0) dy_0 \right\rangle dy dx da dt \\ &= \int \langle v_{\theta}(\cdot), u(\cdot|y_0) \rangle p_{Y_t, X, A}(\cdot|y_0) p_Y(y_0) dy_0 dy dx da dt \\ &= \mathbb{E}_{t \sim \mathcal{U}[0,1], p_Y(y_0), p_{Y_t, X, A|Y_0}(\cdot|y_0)} \langle v_{\theta}(\cdot), u(\cdot|y_0) \rangle. \end{aligned} \quad (19)$$

Finally, because  $u_t(\cdot | y_0)$  does not depend on  $\theta$ , substituting Eqs. (18) and (19) into Eq. (15) and differentiating with respect to  $\theta$  yields:

$$\nabla_{\theta} \mathcal{L}_{\text{FM}}(\theta) = \nabla_{\theta} \mathcal{L}_{\text{CFM}}(\theta). \quad (20)$$

**Proposition 4.2.** *Given a noise sample  $y_1 \sim q(\cdot)$  at  $t = 1$ , the log-density of the resulting potential outcome at  $t = 0$ , obtained via PO-Flow, is given by:*

$$\log \hat{p}_Y(\cdot | x, a, y_1) = \log q(y_1) + \int_0^1 \nabla \cdot v_{\theta}(y(t), t, x, a) dt.$$

*Proof:*

Samples from Continuous Normalizing Flows (CNFs) evolve according to the following Neural ODE:

$$\frac{dy(t)}{dt} = v_{\theta}(y(t), t, x, a), \quad t \in [0, 1], \quad (21)$$

which induces a corresponding evolution of the sample density governed by the Liouville continuity equation:

$$\partial_t p(y, t) + \nabla \cdot (p(y, t) v_{\theta}(y, t, x, a)) = 0. \quad (22)$$

Here,  $p(y, t)$  denotes the time-dependent probability density of the samples  $y$ .

Next, we have that the dynamics of the density  $p(\cdot)$  governed by the velocity field  $v_{\theta}(y, t, x, a)$  is given by:

$$\frac{d}{dt} \log p(y(t), t) = \frac{\nabla p(y(t), t) \cdot \partial_t y(t) + \partial_t p(y(t), t)}{p(y(t), t)} \quad (23)$$

$$= \frac{\nabla p \cdot \partial_t y + \partial_t p}{p} \Big|_{(y(t), t)} \quad (24)$$

$$= \frac{\nabla p \cdot v_{\theta} - \nabla \cdot (p v_{\theta})}{p} \Big|_{(y(t), t)} \quad (\text{by (21) and (22)}) \quad (25)$$

$$= \frac{\nabla p \cdot v_{\theta} - (\nabla p \cdot v_{\theta} + p \nabla \cdot v_{\theta})}{p} \Big|_{(y(t), t)} \quad (26)$$

$$= -\nabla \cdot v_{\theta}. \quad (27)$$

Starting from an initial sample  $y_1 \sim q(\cdot)$  and integrating from  $t = 1$  to  $t = 0$ , we have:

$$\log \hat{p}_Y(\cdot | x, a, y_1) = \log q(y_1) + \int_0^1 \nabla \cdot v_{\theta}(y(t), t, x, a) dt. \quad (28)$$

Besides, if  $q(\cdot)$  is selected as the commonly used  $N(0, I)$ , we have:

$$\log \hat{p}_Y(\cdot | x, a, y_1) = -\frac{d_Y}{2} \log 2\pi - \frac{1}{2} \|y_1\|^2 + \int_0^1 \nabla \cdot v_{\theta}(y(t), t, x, a) dt. \quad (29)$$

## B Experimental Details

### B.1 Synthetic Causal Datasets

Counterfactual outcomes are unobservable in real-world data but can be simulated using synthetic datasets. In our experiments, we evaluate on widely used benchmarks, including the Atlantic Causal

Inference Conference datasets (ACIC 2016 and ACIC 2018), the Infant Health and Development Program (IHDP) [24, 42], and the IBM Causal Inference Benchmark [56].

The ACIC 2016 dataset contains 4,802 samples with 82 covariates each ( $d_X = 82$ ), ACIC 2018 has 1,000 samples with 177 covariates, IHDP includes 747 samples with 25 covariates, and the IBM dataset consists of 1,000 samples with 177 covariates. Each dataset provides three synthetic values per individual: the factual outcome  $y^{(a)}$ , the assigned treatment  $a$ , and the mean potential outcomes under both treatments,  $\mu_0$  (for  $a = 0$ ) and  $\mu_1$  (for  $a = 1$ ).

Moreover, under the following dataset synthesis assumptions: (1) fully specified outcome model  $Y^{(A)} = f(X, A) + \epsilon$ ; (2) shared noise across treatment arms for each individual; and (3) invertibility of the structural function such that, given  $X$ ,  $A$ , and  $Y^{(A)}$ , one can solve for  $\epsilon$  — we can synthesize the counterfactual outcome through the following procedure:

1. **Abduction:** infer the unobserved noise term  $\epsilon'$  from the factual outcome  $Y^{(A)}$ , covariates  $X$ , and treatment  $A$ ;
2. **Action:** intervene by changing the treatment assignment to  $1 - A$ ;
3. **Prediction:** use the inferred noise  $\epsilon'$  and new treatment to compute the counterfactual outcome via  $Y^{(1-A)} = f(X, 1 - A) + \epsilon'$ .

All datasets are generated using diverse simulation mechanisms, and we provide the specific versions used along with our code. For example, the IHDP dataset is generated using 25 covariates and a coefficient matrix  $W$ , following the data-generating process:

$$\begin{aligned} X &\sim \text{Real-world distribution } p_X(\cdot), \\ A &\sim \text{Real-world Treatment assignment based on } X, \\ Y &= A(X\beta - \omega) + (1 - A)\exp((X + W)\beta) + \epsilon, \quad \epsilon \sim N(0, 1). \end{aligned} \tag{30}$$

where  $\beta$ ,  $W$ , and  $\omega$  are parameters defined by the specific simulation setting.

## B.2 Counterfactual Image Experiments

To intuitively visualize PO-Flow’s counterfactual performance and evaluate its effectiveness on high-dimensional data, we train PO-Flow on the latent space of a pre-trained Variational Autoencoder (VAE) [36] using the CelebA dataset.

The CelebFaces Attributes Dataset (CelebA) comprises 202,599 face images, each with a resolution of  $178 \times 218$  pixels. Each image is annotated with 40 binary facial attributes. In our experiments, we selected the male/female attribute as the treatment variable  $A \in \{\text{male}, \text{female}\}$ , and defined covariates  $X \in \mathbb{R}^6$  to represent features such as hair, eyebrows, bangs, and lips.

The VAE is pre-trained on the full CelebA dataset with a 512-dimensional latent space. Each  $178 \times 218$  face image is then encoded into this latent space, yielding the training target  $Y \in \mathbb{R}^{512}$ . PO-Flow is subsequently trained on the triplet  $(Y, X, A)$  to generate counterfactual male face representations given original female faces.

## B.3 Neural Network Structure and Implementation Information

The neural network used in experiments on causal datasets (except the CelebA image task) takes as input  $y(t)$ ,  $x$ ,  $t$ , and  $a$ . The model is composed of the following components: (1) an outcome embedding layer that projects  $y(t)$  to the same dimension as the concatenated  $(x, a)$ ; (2) a FiLM layer that applies feature-wise affine transformations to the embedded  $y(t)$ , conditioned on  $(x, a)$ ; (3) two residual blocks, each consisting of a gated two-layer MLP conditioned on  $(x, a)$ , with residual averaging and skip connections; and (4) a projection layer that maps the final hidden representation to two velocity vectors  $v_0$  and  $v_1$ , corresponding to treatments 0 and 1.

The neural network used for the counterfactual image generation task has an architecture composed of the following components: (1) a conditioning MLP that encodes the pair  $(t, a)$  into a hidden feature vector via two linear layers and a ReLU activation; (2) an input layer that takes the concatenation of  $y(t)$  and  $(t, a)$ , followed by a ReLU-activated linear transformation; (3) four residual blocks, each composed of two linear layers with a ReLU nonlinearity, where the conditioning feature is injected additively at each block; and (4) an output linear layer that maps the final hidden representation back to the latent outcome dimension.

All experiments are conducted on a V100 GPU with 16 GB of memory. The training time for causal datasets (excluding CelebA counterfactual face image generation) depends on the dataset and batch sizes. For example, training on the ACIC 2018 dataset with a batch size of 256 typically takes 2–4 seconds per epoch. Log-density evaluation, as discussed in Section 4.3, involves divergence integration and requires significantly more time than other test metrics.

## B.4 Runge-Kutta numerical integration method

We apply the classical 4th-order Runge-Kutta method to solve the Neural ODE in the forward process of PO-Flow. Given a factual outcome  $y^{(a)}$ , we aim to compute the latent embedding  $z_y = y(1)$  by integrating the velocity field  $v_\theta$  from  $t = 0$  to  $t = 1$ , with initial condition  $y(0) = y^{(a)}$ . Let  $h$  denote the step size, and define discrete time steps  $t_k = kh$ , for  $k = 0, 1, \dots, T$ , such that  $Th = 1$ . The update rule at each step is:

$$y(t_{k+1}) = y(t_k) + \frac{h}{6} (k_1 + 2k_2 + 2k_3 + k_4),$$

where

$$\begin{aligned} k_1 &= v_\theta(y(t_k), t_k, x, a), \quad k_2 = v_\theta\left(y(t_k) + \frac{h}{2}k_1, t_k + \frac{h}{2}, x, a\right), \\ k_3 &= v_\theta\left(y(t_k) + \frac{h}{2}k_2, t_k + \frac{h}{2}, x, a\right), \quad k_4 = v_\theta(y(t_k) + hk_3, t_k + h, x, a), \end{aligned}$$

with  $y(0) = y^{(a)}$  and  $y(1) = z_y$ . This produces a numerically integrated trajectory from the observed sample to its latent representation.

## B.5 Hutchinson trace estimator

The computations of the log-density of the POs involve the calculation of  $\nabla \cdot v_k(x, t)$ , i.e., the divergence of the velocity field represented by a neural network. This may be computed by brute force using reverse-mode automatic differentiation, which is much slower and less stable in high dimensions.

We can express  $\nabla \cdot v_\theta(y, t, x, a) = \mathbb{E}_{\epsilon \sim p(\epsilon)} [\epsilon^T J_v(y)\epsilon]$ , where  $J_v(y)$  is the Jacobian of  $v_\theta(y, t, x, a)$  at  $y$ . Given a fixed  $\epsilon$ , we have  $J_v(y)\epsilon = \lim_{\sigma \rightarrow 0} \frac{v_\theta(y + \sigma\epsilon, t, x, a) - v_\theta(y, t, x, a)}{\sigma}$ , which is the directional derivative of  $v_\theta$  along the direction  $\epsilon$ . Therefore, for a sufficiently small  $\sigma > 0$ , we can propose the following Hutchinson estimator [31, 64]:

$$\nabla \cdot v_\theta(y(t), t, x, a) \approx \mathbb{E}_{p(\epsilon)} \left[ \epsilon \cdot \frac{v_\theta(y(t) + \sigma\epsilon, t, x, a) - v_\theta(y(t), t, x, a)}{\sigma} \right], \quad (31)$$

where  $p(\epsilon)$  is a distribution in  $\mathbb{R}^{d_Y}$  satisfying  $\mathbb{E}[\epsilon] = 0$  and  $\text{Cov}(\epsilon) = I$  (e.g., a standard Gaussian). This approximation becomes exact as  $\sigma \rightarrow 0$ .

## B.6 Adapted Implementation Details for DiffPO and GANITE Counterfactuals

DiffPO was not originally designed for counterfactual tasks. However, since DiffPO uses a diffusion model as its base, we are able to adapt the algorithm to incorporate an "encoding" and "decoding" structure similar to that of PO-Flow. Our adapted implementation of their algorithm for counterfactual estimation is summarized in Algorithm 3.

---

**Algorithm 3:** Adapted DiffPO for Counterfactual

---

**Input:**  $(y^{(a)}, x, a) \sim p_{Y,X,A}(\cdot)$   
1:  $z_0 \leftarrow y^{(a)}$   
2: Forward Process:  
3: for  $t = 0, \dots, T - 1$ :  
4:  $z_{t+1} \leftarrow \sqrt{\frac{\alpha_{t+1}}{\alpha_t}} z_t + f_{\theta}(z_t, t|x, a) \left( \sqrt{1 - \alpha_{t+1}} - \sqrt{\frac{\alpha_{t+1}(1 - \alpha_t)}{\alpha_t}} \right)$   
5:  $z_y \leftarrow z_T$   
6: Reverse Process:  
7: Follow their official implementation in Section 5.3  
8: **Return**  $\hat{y}^{(1-a)} := \hat{y}_0$

---

Similarly, GANITE was not originally designed for counterfactual inference. It consists of a generator and a discriminator, with the final output targeting CATE estimation. However, the generator also produces a proxy counterfactual given the factual input, which we use to evaluate its counterfactual estimation performance.

## C Additional Experimental Results

### C.1 RMSE Convergence

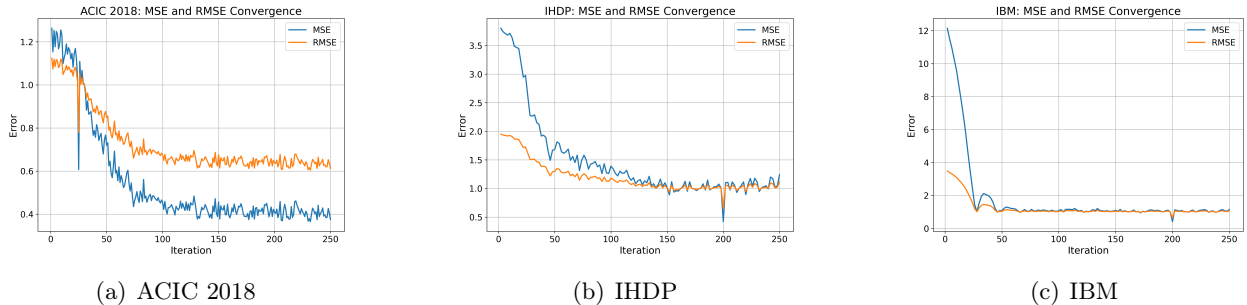


Figure 4: Convergence of MSE and RMSE for predicted potential outcomes over the training iterations on the ACIC 2018, IHDP, and IBM datasets.

PO-Flow demonstrates rapid convergence across datasets, requiring only around 250 training iterations (not epochs) with a batch size of 200 per iteration. This highlights the model’s strong training efficiency.

### C.2 Additional counterfactual images



Figure 5: PO-Flow counterfactual image generation from female to male faces. (a): Each row shows a factual outcome  $y^{(a)}$  (1st column), its encoded latent  $z_y$  (2nd column), and reverse-time decoding at  $t = 2/3$ ,  $t = 1/3$ , and  $t = 0$  (3rd–5th columns), yielding the counterfactual  $\hat{y}^{(1-a)}$ . (b): Counterfactuals decoded from perturbed latents  $z_y + \delta$ , with  $\delta \sim \mathcal{N}(0, 0.2I)$ .